Materials Science & Engineering B 261 (2020) 114660

Contents lists available at ScienceDirect

Materials Science & Engineering B

journal homepage: www.elsevier.com/locate/mseb

Fabrication of three-dimensional PCL/$BiFeO_3$ scaffolds for biomedical applications

Songul Ulag[a,b], Cevriye Kalkandelen[a,c], Tuba Bedir[a,g], Gokce Erdemir[d], Serap Erdem Kuruca[e], Fatih Dumludag[f], Cem Bulent Ustundag[g], Erkan Rayaman[h], Nazmi Ekren[a,i], Beyhan Kilic[a,j], Oguzhan Gunduz[a,k,*]

[a] Center for Nanotechnology & Biomaterials Application and Research (NBUAM), Marmara University, Istanbul 34722, Turkey
[b] Department of Metallurgical and Materials Engineering, Institute of Pure and Applied Sciences, Marmara University, Istanbul 34722, Turkey
[c] Vocational School of Technical Sciences, Istanbul University-Cerrahpasa, Istanbul 34452, Turkey
[d] Department of Molecular Medicine, Aziz Sancar Institue of Experimental Medicine, Istanbul University, Istanbul 34452, Turkey
[e] Department of Physiology, Faculty of Medicine, Istanbul University, Istanbul 34452, Turkey
[f] Department of Physics, Faculty of Sciences and Arts, Marmara University, Istanbul 34722, Turkey
[g] Department of Bioengineering, Faculty of Chemical and Metallurgical Engineering, Yildiz Technical University, Istanbul 34220, Turkey
[h] Department of Pharmaceutical Microbiology, Marmara University, Istanbul 34722, Turkey
[i] Department of Electrical and Electronics Engineering, Faculty of Technology, Marmara University, Istanbul 34722, Turkey
[j] Department of Electrical Engineering, Faculty of Electrical and Electronics, Yildiz Technical University, Istanbul 34220, Turkey
[k] Department of Metallurgical and Materials Engineering, Faculty of Technology, Marmara University, Istanbul 34722, Turkey

ARTICLE INFO

Keywords:
Bismuth ferrites
Co-precipitation method
Conductivity
Dielectric constant
Multiferroics
3D printing process

ABSTRACT

The aim of this study is to examine the pH effect on bismuth ferrite ($BiFeO_3$) properties and observe the $BiFeO_3$ behaviour in the polycaprolactone (PCL). In this paper, $BiFeO_3$ was synthesized via co-precipitation method at three different pH values (10.64, 11.32, and 11.58). These produced particles were added into the 25wt.%PCL solutions separately to get the scaffolds using a 3D printing process. Crystallite sizes were determined from the Debye-Scherer formula using XRD. With different pH values, crystal sizes were found as 15, 12, and 10 nm and particle sizes determined from SEM were 142, 134, and 111.39 nm for 10.64, 11.32, and 11.58, respectively. The adenocarcinoma lung cancer cell (A549) adhesion on the scaffolds revealed that cells could attach to the scaffolds. Maximum dielectric constant values were obtained for the pellets and scaffolds as 10.37 nF and 6.16 nF for the pellet $BiFeO_3$ (pH = 11.58) and the scaffold 25wt.%PCL/2wt.%$BiFeO_3$ (pH = 11.58), respectively.

1. Introduction

In recent years, materials that have both electrical and magnetic properties have taken attention in research due to their controllable property to create novel devices. These materials called multiferroic materials that display the simultaneous effects of ferromagnetism, ferroelectricity, and ferroelasticity, etc. These properties are due to the coupled electric, magnetic, mechanical and structural properties [1,2]. The capability of ferroelectricity and anti-ferromagnetic is a unique property of Bismuth ferrite ($BiFeO_3$, BFO) which is a single-phase multiferroic material that has a polar R3c space group with rhombohedral distorted cell [3,4]. Bi lone pair $6s^2$ electrons provide to ferroelectricity and G-type antiferromagnetism caused by the stereochemical activity of the partially filled 3d orbital of the Fe^{3+} ions. It is known that d-shells are an essential property for showing magnetism. These d-shells are normally empty for ferroelectric systems. Since $BiFeO_3$ is multiferroic at room temperature, it is an open candidate for device applications. Another application of BFO is THz radiation emission, which is of great interest for many applications from telecommunications to security. A significant advantage of using this material is that it is lead-free. This material has the potential for many areas such as four-state memory and in spintronic, ferroelectric memories, storage, and piezoelectric devices due to its interesting physical properties [5]. The electrical and magnetic properties of the $BiFeO_3$ materials have been studied in detail [6]. Another field of application is biomedical engineering. In a study by Biswas et al., the antibacterial activity of Bismuth ferrite material against *Staphylococcus aureus* was tested. BFO showed significant antibacterial activity against this bacteria [7]. In another study, Staedler et al. investigated cell compatibility and cytotoxicity specificity of Bismuth ferrite nanoparticles. The results

* Corresponding author.
E-mail address: ucemogu@ucl.ac.uk (O. Gunduz).

https://doi.org/10.1016/j.mseb.2020.114660
Received 22 March 2020; Received in revised form 4 June 2020; Accepted 20 July 2020
Available online 05 August 2020
0921-5107/ © 2020 Elsevier B.V. All rights reserved.

support the attractiveness of functional $BiFeO_3$ to biomedical applications that focus on advanced diagnostic imaging [8]. Bismuth ferrite can be synthesized with many techniques which are the solid-state method, mechanochemical method, sol-gel method, hydrothermal method, and sonomechanical method. However, some of these techniques are required high temperature for annealing plans [9]. Also, these techniques can cause the formation of other phases which can be Bi_2O_3 and $Bi_2Fe_4O_9$. Several studies have been performed, which produce the $BiFeO_3$ with co-precipitation method.

In Xie et al. study, $BiFeO_3$ was produced with the co-precipitation method, and they synthesized three single-phase bismuth ferrites ($BiFeO_3$, $Bi_{25}FeO_{40}$, $BiFeO_9$) [10]. Munesswaran et al. work examined the pH effect on structural, chemical, morphological, and dielectric properties by producing $BiFeO_3$ with three different pH values. They synthesized nanosized multiferroic $BiFeO_3$ (BFO) powders successfully with the co-precipitation method [11]. Sangian et al. used a reverse chemical co-precipitation method to produce the $BiFeO_3$ nanoparticles. They also investigated the effects of different pH values on magnetic and microstructural properties [6]. There are many studies about the electrical, magnetic, morphological and structural properties of bismuth ferrite nanoparticles [1–6]. Several studies have also been conducted in biomedical applications [8,12]. However, three-dimensional scaffolds formed with bismuth ferrite particles and their characteristics behaviours within the 3D-printed scaffolds were not investigated. This study is aimed to be a pioneer in this aspect and can note that bismuth ferrite is an ideal candidate for biomedical applications as a nanofiller.

In this present study, the co-precipitation method was used for $BiFeO_3$ synthesis which method provides rapid and simple preparation, controllable particle size and composition, needs low temperature at the synthesizing process compared to the other methods [5,13]. Polycaprolactone was used as a matrix material of the scaffolds which is a synthetic polymer that has many advantages in biomedical applications such as biocompatible properties, slow biodegradation characteristics [14] and porous structure [15]. $BiFeO_3$, $BiMnO_3$, and $ReMnO_3$ are the principal multiferroic perovskite oxides studied so far. Through these materials, the Neel (370 °C) and Curie (830 °C) temperature values of the $BiFeO_3$ are higher than others, and it has superior potentials for memory machines, sensors, and optical filter sand smart devices [11]. As a result, $BiFeO_3$ with three different pH values and 3D-printed 25% PCL/2%$BiFeO_3$ scaffolds with three different pH values were analyzed in detail in this study to compare the structural, dc/ac conductivity, dielectric properties and biological properties for both particles and scaffolds.

2. Materials and method

2.1. Materials

Iron (III) nitrate nonahydrate ($Fe(NO_3)_3$, MW = 403.95 g/mol), Bismuth (III) nitrate ($Bi_5O(OH)_9(NO_3)_4$, MW = 1.461,99 g/mol), Dichloromethane (DCM), and Nitric acid (65%) were purchased from Merck KGaA, Germany. Ammonia Solution (25%, MW = 35.05 g/mol) was bought from ISOLAB (Wertheim, Germany). Polycaprolactone (PCL, MW = 80.000) was purchased from Sigma Aldrich (United Kingdom). Distilled water supplied by water distiller (Liston).

Testing Microorganisms; Staphylococcus aureus ATCC 29213, Escherichia coli ATCC 25922, Pseudomonas aeruginosa ATCC 27853, Candida albicans ATCC 90028. Medium; Mueller Hinton agar (Merck) for bacteria, Sabouraud dextrose agar (SDA) (Merck) for yeasts, ethanol was used as the solvent of the samples. Control Groups; Meropenem was used for bacteria, and amphotericin B was used for C. Albicans.

2.2. $BiFeO_3$ synthesis by co-precipitation method

Co-precipitation is an effective method for producing nano-scaled magnetic particles to get precursors by simultaneous precipitation of two cations (Bi^{3+}, Fe^{3+}). In this study, $BiFeO_3$ nanoparticles were synthesized with this method. Firstly, 2.58 g iron nitride ($Fe(NO_3)_3{\cdot}9H_2O$) was dissolved in the distilled water (10 ml) at the magnetic stirrer with 300 rpm for 15 min. Then, 1.86 g bismuth nitride ($Bi(NO_3)_3.5H_20$) was solved in the 10 ml nitric acid for half an hour at the stirrer with the same rpm. After two solutions were dissolved entirely, two solutions were mixed at the same beaker for 15 min to obtain a homogeneous mixture. When the transparent mixture obtained, the ammonia solution was added into the mix to control the pH to get a precipitate. The preparation of the precursor and co-precipitation solutions was performed at room temperature. Three different pH values were studied, which were 10.64, 11.32, 11.58 to examine the pH values on the properties of the powder's particle size. The resulting precipitate was passed through the filter paper and washed with distilled water to remove the toxic effect of agents. Then, the powders put in the oven for 24 h at 100 °C and they were calcinated at 550 °C for 3 h to obtain crystallize and pure bismuth ferrite.

2.3. Preparation of the solutions

Firstly, 2.5 g PCL was solved in 10 ml DCM to obtain 25%PCL solutions as a control group, and this solution was put at the magnetic stirrer for an hour with 300 rpm. Three different pH values of $BiFeO_3$ (2%) were individually blended with 25%PCL solutions under the same stirring rpm at ambient temperature for half an hour to print.

2.4. 3D printing of 25%PCL and 25%PCL/2%$BiFeO_3$ scaffolds

3D-Printing device (modified Ultimaker 2+) was used for fabrication of 25%PCL and 25%PCL/2%$BiFeO_3$ scaffolds. First of all, the 3D model was drawn using the Solidworks program with $20 \times 20 \times 0.3\ mm^3$ dimensions. The process parameters were adjusted depending on the solutions. 25%PCL had a clear, transparent structure, which was easy to optimize the process parameters. The nozzle diameter was 0.4 mm, the infill rate was 70%, and the extrusion multiplier was 0.3% for 25%PCL scaffolds. The nozzle diameters were 0.4, 0.3, and 0.25 mm, extrusion multiplier values were 0.8, 0.5, and 0.3 for 25%PCL/2%$BiFeO_3$ (10.64), 25%PCL/2%$BiFeO_3$ (11.32), and 25% PCL/2%$BiFeO_3$ (11.58), respectively. The $BiFeO_3$ particles were labelled as particle PA, PB, and PC and correspond to pH values, 10.64, 11.32, and 11.58, respectively. The scaffolds were labelled as scaffold SU (undoped), and scaffolds doped with $BiFeO_3$ (with pH 10.64, 11.32, and 11.58) and were labelled as scaffold SA, SB, and SC, respectively (Table 1). All scaffolds were infilled with a ratio of 70%. After the printing process, the scaffolds were ready to characterize in addition to the $BiFeO_3$ powders with three different pH values.

2.5. Characterization of the nanoparticles and 3D-printed scaffolds

Fourier Transform Infrared Spectroscopy (FT-IR) were recorded with JASCO-4000 FT-IR spectroscopy at 4000–400 cm^{-1} scanning range with 4 cm^{-1} resolution. Morphological characterization of the pure nanoparticles and the printed scaffolds was examined by an SEM (MA-EVO10, ZEISS). The energy dispersive spectroscopy (EDS) was

Table 1
The properties and label of the samples.

Samples	Codes
$BiFeO_3$ (pH:10.64)	Particle A (PA)
$BiFeO_3$ (pH:11.32)	Particle B (PB)
$BiFeO_3$ (pH:11.58)	Particle C (PC)
25%PCL	Scaffold undoped (SU)
25%PCL/2%$BiFeO_3$ (pH:10.64)	Scaffold A (SA)
25%PCL/2%$BiFeO_3$ (pH:11.32)	Scaffold B (SB)
25%PCL/2%$BiFeO_3$ (pH:11.58)	Scaffold C (SC)

taken for all $BiFeO_3$ nanoparticles. Quorum SC7620 was used for the coating of the powders and scaffolds with the Au element for the 60s. DSC was used for determining of thermal characterization of both nanoparticles and printed scaffolds by a Shimadzu DSC-60 Plus machine. The temperature range of the device ranges from 25 °C to 600 °C, and this temperature range was used in this study with a heating rate of 10 °C/min. XRD device was used to determine the crystal structure of $BiFeO_3$ powders with a Cu source (λ = 1.54060 A°). The acquisition parameters of the XRD system were adjusted to 40 kV, 30 mA, the scan range of 10–90°, 0.48 (°/min) scan speed, and preset time was 2 sec. The crystallite size can be calculated by measuring the full width at half maximum (FWHM) using Debye-Scherrer formula (2.1):

$$DXRD = \frac{k.\lambda}{\beta.\cos\theta} \quad (2.1)$$

D_{XRD} represents the crystallite size in nm scale, k is the shape factor (0.89), β is the FWHM (radian), λ is the wavelength of the X-rays, and θ shows the Bragg's diffraction angle (°) [16].

To clarify the effects of pH values of the starting solution of $BiFeO_3$ on electrical properties of the $BiFeO_3$ pellets, circular Silver (Ag) metal electrodes were deposited onto both surface of the disk of the pellets in thermal evaporation system (Edwards Auto 500) in high vacuum ambient ($< 10^{-6}$ mbar). Radius and thickness of the metal electrodes were 2.5 mm and 1500 Å, respectively. The thickness of the metal electrodes was measured using film thickness monitor FTM7. Electrical contacts were made by using silver paste. Electrical measurements were also done on the scaffolds. The scaffolds were placed between two circular silver disks with radius 3.5 mm to determine their dc and ac conductivity and dielectric properties. Electrical measurements were performed in a homemade aluminium chamber at room temperature (295 K). To prevent the samples from the effects of the gases took placed in the air, the measurements were performed in a vacuum ($< 10^{-2}$ mbar). To investigate effects of the pH values of the starting solution on DC and AC conductivity and dielectric properties of the $BiFeO_3$ pellets and scaffolds, three different pellets, synthesized from the starting solutions with different pH values, and four different scaffolds (undoped and three different scaffolds doped with different $BiFeO_3$, synthesized from the starting solutions with varying values of pH) were prepared. DC electrical properties of the pellets and scaffolds were investigated utilizing current-voltage (I–V) measurements at 295 K using Keithley model 6517B programmable electrometer. AC electrical measurements of the pellets were performed in the frequency range of 40 Hz–100 kHz at the same temperature using Keithley model 3330 LCZ meter. All measurements were carried in dark ambient, and the measurement system was computerized.

Bismuth nanoparticle effects on A549 (human adenocarcinoma) lung cancer cell line was tested *in vitro* to observe the $BiFeO_3$ capability on biomedical studies [12,17]. A549 lung cancer cell line was obtained from American Type Culture Collection (ATCC). Cells were cultured in Dulbecco's modified Eagle medium (DMEM, Gibco) with 10% Fetal bovine serum (FBS, Gibco) and 1% penicillin/streptomycin in a 5% CO_2 humidified air incubator, maintained at 37 °C. When the cells reached 80% of confluence, they were washed with PBS and trypsinized with 0.25% Trypsin-EDTA for passaging and seeding each time. The confluent cells were used in cytotoxicity tests and SEM investigations. Firstly, the conditioned medium was prepared to understand any possible toxic effect induced by possible ionic leach-out products from the samples into the medium. For this aim, a 3 ml fresh medium was added in tubes with a piece (~0,05 g) of tested material (PCL composites) which were kept in the incubator. 3 days after the conditioned medium was extracted and later used in cytotoxicity tests. MTT assays were performed in 96-well plates. A549 cells (about 10^5 cells per well) were seeded onto the 4 h UV sterilized polymers and incubated for 3 days. Cell viability was measured by determining mitochondrial NADH/NADHP–dependent dehydrogenase activity, which resulted in the cellular conversion of the 3-(4, 5-dimethylthiazol-2-gl)-5-(3-carboxymethoxylphenyl)-2-(4-sulfophenyl-2H) tetrazolium salt into a soluble formazan dye. After 3 days, supernatants were removed, and 10 µl 3-{4, 5-dimethylthiazol-2yl}-2,5-diphenyl-2H-tetrazolium-bromide (MTT-5 mg/ml-Sigma) solution was added to each well. Following incubation at 37 °C for 3.5 h and kept dark in a humidified atmosphere at 5% CO_2 in the air. MTT was taken up by active cells and reduced in the mitochondria to an insoluble purple formazan granule [18]. Subsequently, the supernatant was discarded, and the precipitated formazan was dissolved in dimethyl sulfoxide (100 µl per well), and optical density of the solution was evaluated using a microplate spectrophotometer (Kayto RT-2100C) at a wavelength of 570 nm. The specimens were placed in the 6-well cell culture plates and sterilized for 4 h. A549 cells were seeded in these plastic dishes and incubated for 24 h in a humidified incubator at 37 °C with 95% air and 5%CO_2. At the end of 24 h, the media were removed, and specimens were fixed with 3% volume fraction of glutaraldehyde, subjected to graded (30–100%) alcohol dehydration and kept at −20 °C.

In the F-actin staining, the A549 cells were seeded at 5×10^3 cells/cm^2 on the scaffolds in the 6 well plate. After A549 proliferation on the scaffolds for 3 days, the F-actin staining kit (Abcam, CytoPainter F-actin Labeling Kit) was carried out to observe the cell phenotype according to manufacturer protocol. Firstly, the cells were initially fixed with 4% formaldehyde (Sigma) at room temperature for 15 min, washed and incubated with 0.1% Triton X-100 (Merck) to increase permeability for 10 min. The cells were further incubated with green fluorescent phalloidin conjugate for 1 h at room temperature. After that, the cell-scaffold constructs were washed with PBS and incubated with DAPI (Invitrogen) (1:5000) for 10 min at room temperature for nuclei staining. Final washing of the constructs was done with PBS before mounting on a glass slide and visualized under laser scanning confocal microscopy (LSM 700, Zeiss).

Microorganism suspensions were prepared from colonies on solid medium in 0.85% physiological saline (FTS). Bacterial suspensions were adjusted to a concentration of 108 CFU/ml and yeast suspensions of 106 CFU/ml according to the Mc Farland 0.5 standard turbidity [19]. 0.1 ml of these suspensions were taken and spread on the prepared surface of the prepared 4 mm thick medium with a sterile swab. For the gutter diffusion method, 50 µl of sample and control solutions (meropenem (10 µg/canal) for bacteria, amphotericin B (100 µg/canal) for C. Albicans were opened into the gutters by opening 5 mm diameter canal on microorganism spreading media with the help of sterile Pasteur pipette. For the disc diffusion method, microorganism spread media was disc-discovered, and meropenem antibiotic disc was placed for bacteria. Petri dishes were incubated for 18–24 h at 350 °C for bacteria growth and 24–48 h at 350 °C for the growth of yeasts. Reproduction inhibition zones were measured in mm at the end of time. The labels of the samples were given in Table 2 for the antimicrobial test.

3. Results and discussions

The FTIR spectrums of the nanoparticles derived from the co-precipitation and fabricated 3D-printed scaffolds were shown in Fig. 1. In Fig. 1 (A, a), there were observed several absorption peaks at

Table 2
Samples with their labels for the antimicrobial test.

Sample Number	Label Information
1	PCL/$BiFeO_3$ (11.58) (powder and disc)
2	PCL/$BiFeO_3$ (11.32) (powder and disc)
3	PCL/$BiFeO_3$ (10.64) (powder and disc)
4	PCL (disc)

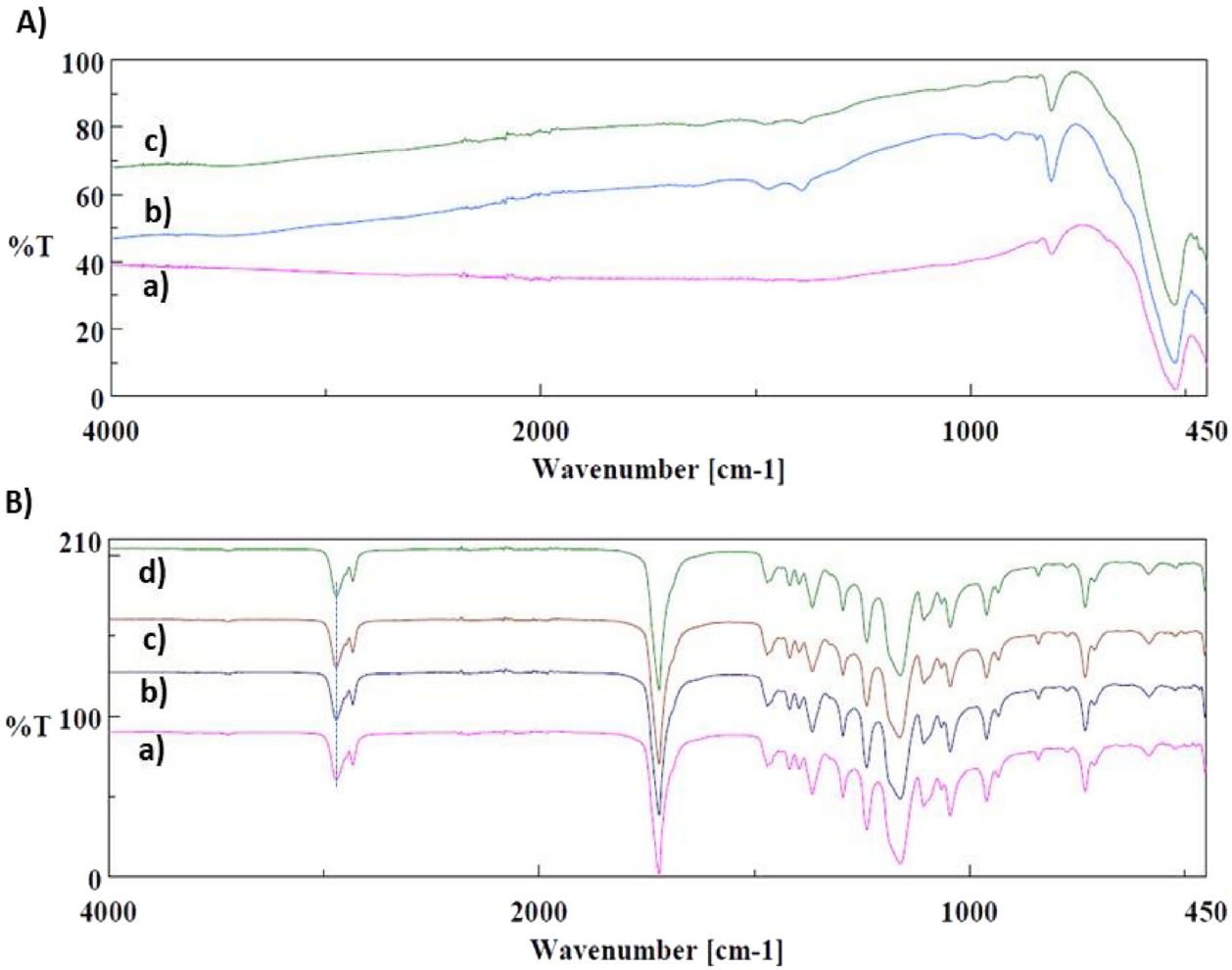

Fig. 1. FTIR spectrums of the synthesized powders and printed scaffolds: PA (A, a), PB (A, b), PC (A, c); SU (B, a), SA (B, b), SB (B, c), and SC (B, d).

~2369.1 cm^{-1}, ~2161.8 cm^{-1}, ~810.9 cm^{-1}, ~525.5 cm^{-1}, ~450.3 cm^{-1} for PA. The peak at ~810.9 cm^{-1} was due to the variation of NO_3^-. The bands which are characteristic peaks of ferrite were detected in the range of 450–525 cm^{-1}. These peaks are related to metallic ions [20]. The bands at ~2161.8 cm^{-1} and ~2369.1 cm^{-1} can be due to the CO_2 chemical compound and trapped NO_3^- ion present in the powder [21]. Fig. 1(A, b) showed the absorption peaks of the PB which were ~1393.3 cm^{-1}, ~811.9 cm^{-1}, ~523.6 cm^{-1}, and ~450.3 cm^{-1}. The peak observed at ~1393.3 cm^{-1} is related to the NO_3^- stretching vibrations [22]. There were seen three main peaks at ~811.9 cm^{-1}, ~525.5 cm^{-1}, ~450.3 cm^{-1} for PC. The band around 523–525 cm^{-1} was linked with the stretching vibration of metal at tetrahedral sites, the other band (450 cm^{-1}) was due to the specific stretching vibration of metal at octahedral sites [20]. $BiFeO_3$ had these characteristic peaks, and they were observed for all particles which had different pH values. In Fig. 1B, FTIR spectrums of the PCL and $BiFeO_3$ doped scaffolds were given. 25%PCL (SU) had main absorption peaks at ~2941.9 cm^{-1} (asymmetric CH_2 stretching), ~2864.7 cm^{-1} (symmetric CH2 stretching), ~1721.2 cm^{-1} (carbonyl stretching), ~1293 cm^{-1} (C–O and C–C stretching) and at ~1238.1 cm^{-1} (C–O–C stretching) (Fig. 1(B, a)) [17]. The $BiFeO_3$ added spectrums had nearly the same absorption peaks with SU. This can be due to the small amount of $BiFeO_3$ into the SU. As a result, the FTIR spectrum of the pure particles showed that there were observed characteristic vibrations of the obtained $BiFeO_3$ powders.

Fig. 2(a–c) displayed SEM images of bismuth ferrite nanoparticles with their EDS spectrums. As shown, $BiFeO_3$ particles with three different pH values, had nearly uniform particle sizes and shapes. By using SEM images, ten different particles were selected, and their particle sizes were measured to get the mean particle value for all nanoparticles. Mean particle sizes were found as 142 ± 22, 134 ± 25, and 111 ± 25 nm for 10.64, 11.32, and 11.58 pH values, respectively. It was said that upon the increase of pH values, the particle size was found to decrease. Elemental analysis showed that Bismuth was seen in all nanoparticles at 69, 57.69, and 75.93 (wt.%) for 10.64, 11.32, and 11.58 pH values. Fe element was seen for 11.32 and 11.58 values at 12.86 and 8.3 (wt.%), respectively.

SEM was applied to assess morphology and pore size of 3D-printed scaffolds. Fig. 3 showed that pores had a nearly uniform distribution. In Fig. 3a, it was observed a rectangular pore shape for SU, and it had 223.92 μm mean horizontal pore size value (Fig. 3b). In Fig. 3c, SA had irregular pore distribution with 203.26 μm mean horizontal pore size value (Fig. 3d). The more uniform pore structure was observed for the SB (Fig. 3e), and it also had a smaller horizontal pore size than SA (Fig. 3f). In Fig. 3g, pore shape nearly circular shape for the SC, and it had the smallest horizontal pore size (Fig. 3h). These variations can be caused by pH effect on scaffolds which decreased the size of the nanoparticles. As a result, it can be said that 3D printing is an effective process to obtain well organized and regular structures [23].

The DSC curve of $BiFeO_3$ powders synthesized from the co-precipitation method at 550 °C was shown in Fig. 4(A). The same thermal behaviours were detected from the curves. The Neel temperature of the pure $BiFeO_3$ powders is ~370 °C [23]. Spectrums showed exothermal peaks at 237 °C, 243 °C, and 231 °C for pH value of 10.64, 11.32, and 11.58, respectively which can represent the mass loss due to the decomposition of $Fe(OH)_3$ and $Bi(OH)_3$ to a metastable state and the

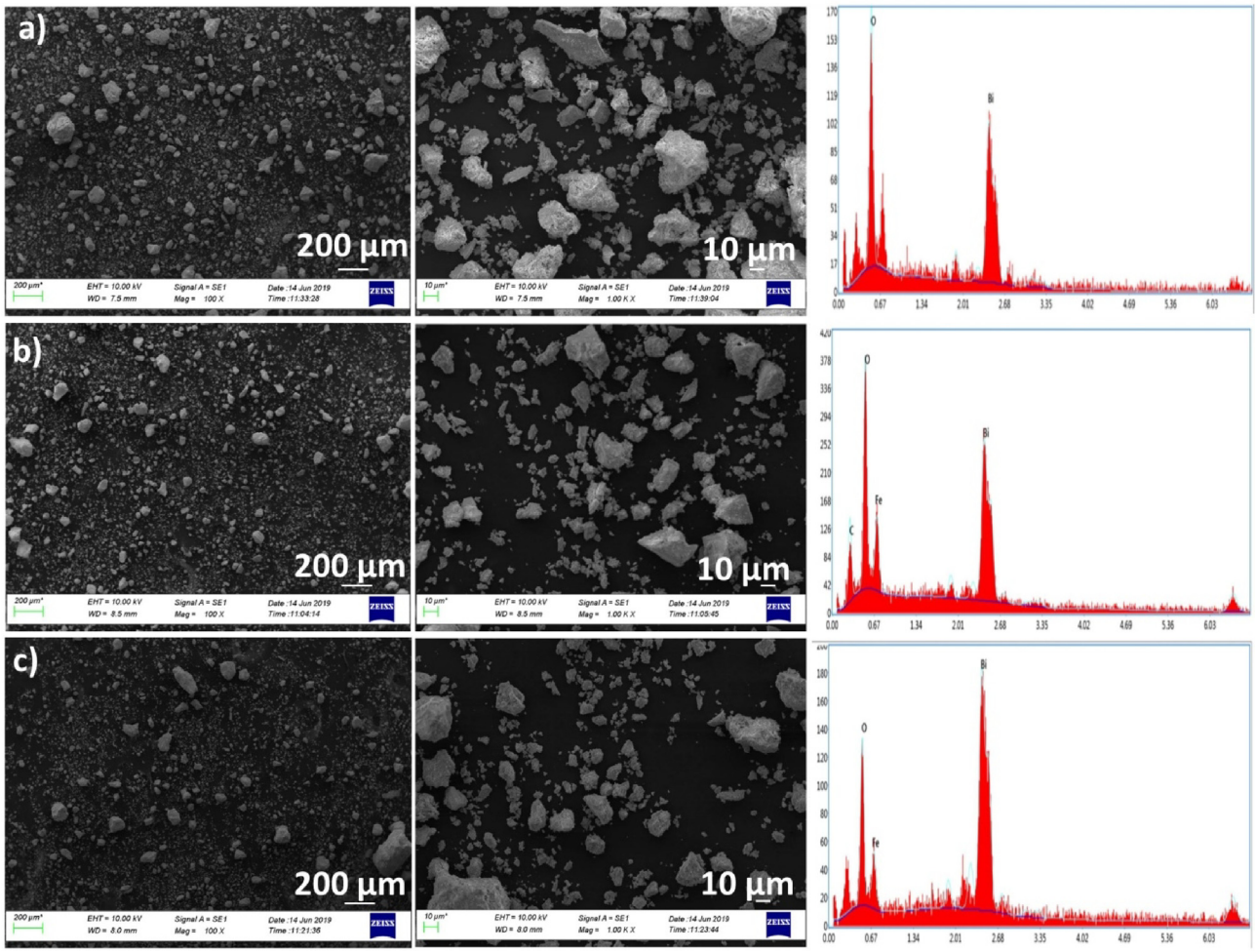

Fig. 2. SEM images of the $BiFeO_3$ particles and their EDS spectrums; pH:10.64 (a, b), pH:11.32 (c, d), and pH:11.58 (e, f).

formation of Bi_2O_3, Fe_2O_3 phases [20]. Other tiny peaks observed at 592 °C (PA), 573 °C (PB), and 591 °C (PC). These peaks can also show the mass loss, which can be the final decomposition temperature of Bi_2O_3, Fe_2O_3 phases [20]. Curie temperature (830 °C) which is assigned to ferroelectric to paraelectric phase conversion of the $BiFeO_3$ was not observed due to the upper-temperature limit (600 °C) of the DSC device.

DSC demonstrated the influence of $BiFeO_3$ content on thermal transition points of the PCL. As seen in Fig. 4(B, a), the melting temperature of the SU was observed at 62 °C and PCL degradation firstly started at ~280 °C and continued up to 530 °C. With $BiFeO_3$ addition, the melting temperature of the 25%PCL was changed from 62 to 60 °C. The peaks at 440 °C, 415 °C, and 400 °C for pH values of 10.64, 11.32, and 11.58, respectively were observed at PCL based composites which indicated that $BiFeO_3$ affect the thermal transition points of the polymer matrix.

XRD analysis was performed to determine the crystalline phases of the nanoparticles. Fig. 5a showed the XRD patterns of $BiFeO_3$ nanoparticles, which had different pH values. There were observed nearly the same characteristic peaks for all particles. Sharp and high peaks prove the excellent crystallinity of the co-precipitation synthesized $BiFeO_3$ nanoparticles, and low-intensity peaks show the presence of the secondary phases such as $Bi_2Fe_4O_9$, $Bi_{25}FeO_{40}$, and $Bi_{36}Fe_{24}O_{57}$ [24,25]. The first peak observed at $2\theta = 22.5^{\circ}$ for all powders. Another peak at $2\theta = 27^{\circ}$ with low intensity represented the Bi_2FeO_9 phase and it had (1 2 0), (1 2 1), and (2 1 1) crystal planes [26]. The observed peaks in the patterns could be specified to be rhombohedra distorted perovskite structure of $BiFeO_3$ with space group R3c [26]. The average particle sizes were calculated from Scherrer formula and determined crystallite sizes were found to be ~15 ± 0.27, 12 ± 0.19, 10 ± 0.32 nm for pH 10.64, 11.32, and 11.58, respectively. The values of the average particle size obtained by SEM (D_{SEM}) were more significant than the crystallite size obtained by the Scherrer formula (D_{XRD}). The reason for this difference can be occurred due to the aggregation of the particles [25]. Crystallite size obtained from Scherrer's formula is the apparent or mean value for powders. This is true for partially crystalline powders and agglomerated powders consisting of smaller primary particles. Moreover, powders generally not monodisperse and contain a size distribution. Therefore, the polydispersity of nanopowders is not considered in Scherrer's formula [27].

XRD analysis was performed to determine the crystalline state of the PCL/$BiFeO_3$ scaffolds as a function of pH values (Fig. 5b). SU had two main diffraction peaks at ~21 and ~23°. These distinct peaks represent the pure PCL polymer peaks which showed that produced SU was highly crystalline [28,29]. There were observed some peaks of $BiFeO_3$ with low and sharp intensities. The peak at ~33° is the characteristic peaks of $BiFeO_3$ and it had low-intensity value in PCL matrix polymer. Another low peak at 83° of $BiFeO_3$ seen in all composite scaffolds. Other peaks of $BiFeO_3$ nanoparticles at ~38° and ~78° had higher intensity values compared to the other peaks. The characteristic peaks observed at range from ~46° to ~66° for $BiFeO_3$ nanoparticles were seen in composite scaffolds with very low-intensity values. When the pH effect with three different values is examined, there was not observed a significant difference between them in XRD spectra. All $BiFeO_3$ added scaffolds with various pH values had nearly the same spectrum. As shown, the crystallinity of SU did not decrease significantly with $BiFeO_3$ addition at different pH values in the $BiFeO_3$ doped scaffolds. The

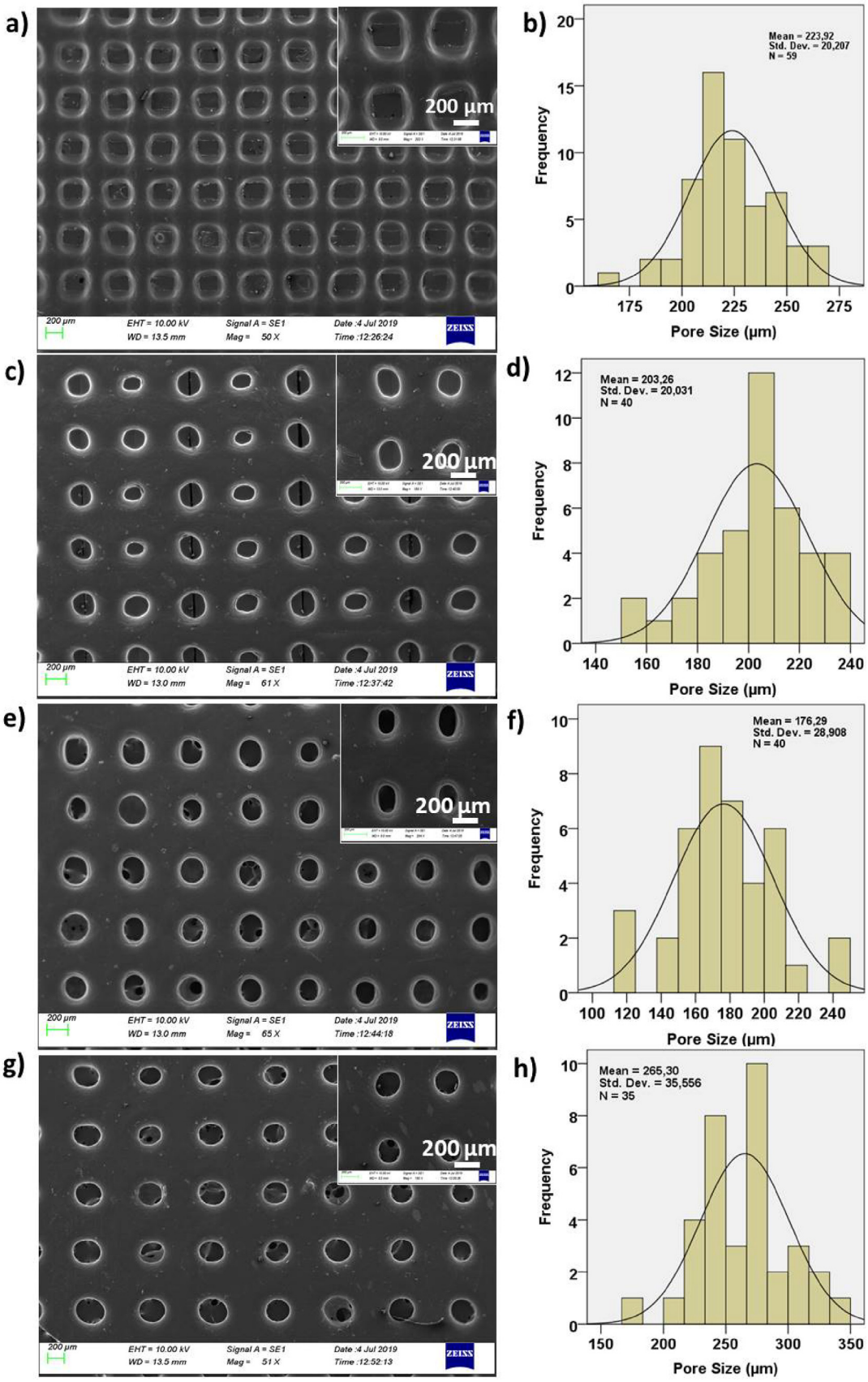

Fig. 3. SEM morphologies and pore size histogram of the SU (a, b), SA (c, d), SB (e, f), and SC (g, h).

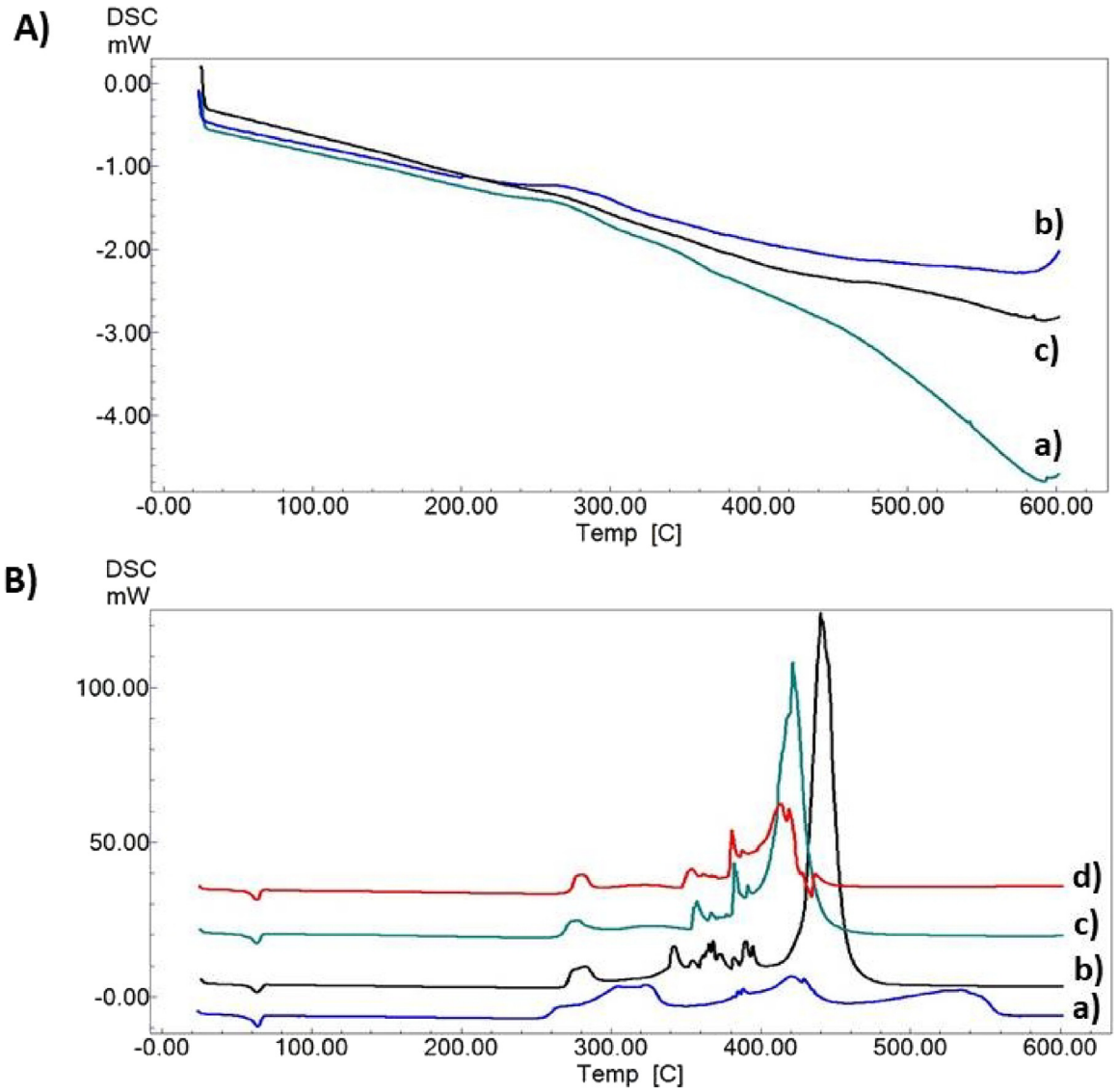

Fig. 4. DSC thermograph of the $BiFeO_3$ nanoparticles: pH value of 11.32 (A, b), 11.58 (A, c), 10.64 (A, a); and 3D-printed scaffolds: SU (B, a), SA (B, b), SB (B, c), and SC (B, d).

observed characteristic peaks of $BiFeO_3$ nanoparticles at composite scaffolds indicated that particles were dispersed in the polymer matrix effectively.

Fig. 6a showed the schematic setup of the AC/DC electrical measurements. DC electrical measurements were performed at room temperature (295 K). To prevent the samples from the effects of the gases took placed in the air, the measurements were performed in a vacuum ($< 10^{-2}$ mbar). Three different pellets obtaining from three different particles were prepared to investigate the effects of the pH values of the starting material on DC conductivity properties.

I-V measurements of the pellets and scaffolds showed ohmic behaviour. DC conductivity values of the pellets were calculated as 5.80×10^{-11}, 9.91×10^{-12}, 1.81×10^{-11} S/m, for the pellets PA, PB, and PC, respectively at 295 K. Fig. 6b showed dc conductivity values of the pellets PA, PB, PC and scaffolds SU, SA, SB, and SC. As seen from the figure that increased pH values caused to decrease dc conductivity values toward the pH values of 11.32 then generated to slight increase toward 11.58. The variation can be attributed to the variation of particle size. From the Fig. 2a–c, keeping in mind that particle size of pH 11.32 and pH 11.58 quite close to each other, we can conclude that although particle sizes were not uniform, in general, particle size decreased. It is known that resistance of the material along the conduction path increases with increasing total grain boundary resistance. Because of particle size decreased, the total number of grains increased and that caused to increase in total grain boundary resistance and that results in conductivity of the material along the conduction path decreased. We can conclude that grain boundary resistance controls the electron flows along with the material. Our results are in agreement with previous reports [30,31]. Fig. 6b also showed dc conductivity values of the scaffolds SU, SA, SB, and SC. DC conductivity values of the scaffolds were calculated as 1.39×10^{-11}, 1.7×10^{-11}, 1.23×10^{-11}, and 1.76×10^{-11} S/m for the scaffolds SU, SA, SB, and SC, respectively at 295 K. As seen from the figure conductivity of the scaffolds varied in a narrow band and variation of conductivity of the scaffolds showed similar behaviour with that of pellets.

AC electrical measurements were performed in the frequency range of 4×10^{-2}–100 kHz, at room temperature (295 K) and in a vacuum as mentioned above. In this part, the effects of pH of the starting solutions of the $BiFeO_3$ on i) ac conductivity (σ_{ac}), and ii) frequency dependence ac conductivity of the pellets and scaffolds were investigated. To do this, ac conductivity values of the samples were measured as a function of frequency (f). Fig. 6c showed ac conductivity values (Log σ_{ac}) of the pellets PA, PB, PC and scaffolds SU, SA, SB, and SC with their fitting lines between the frequencies 10–100 kHz at 295 K, in a vacuum in the

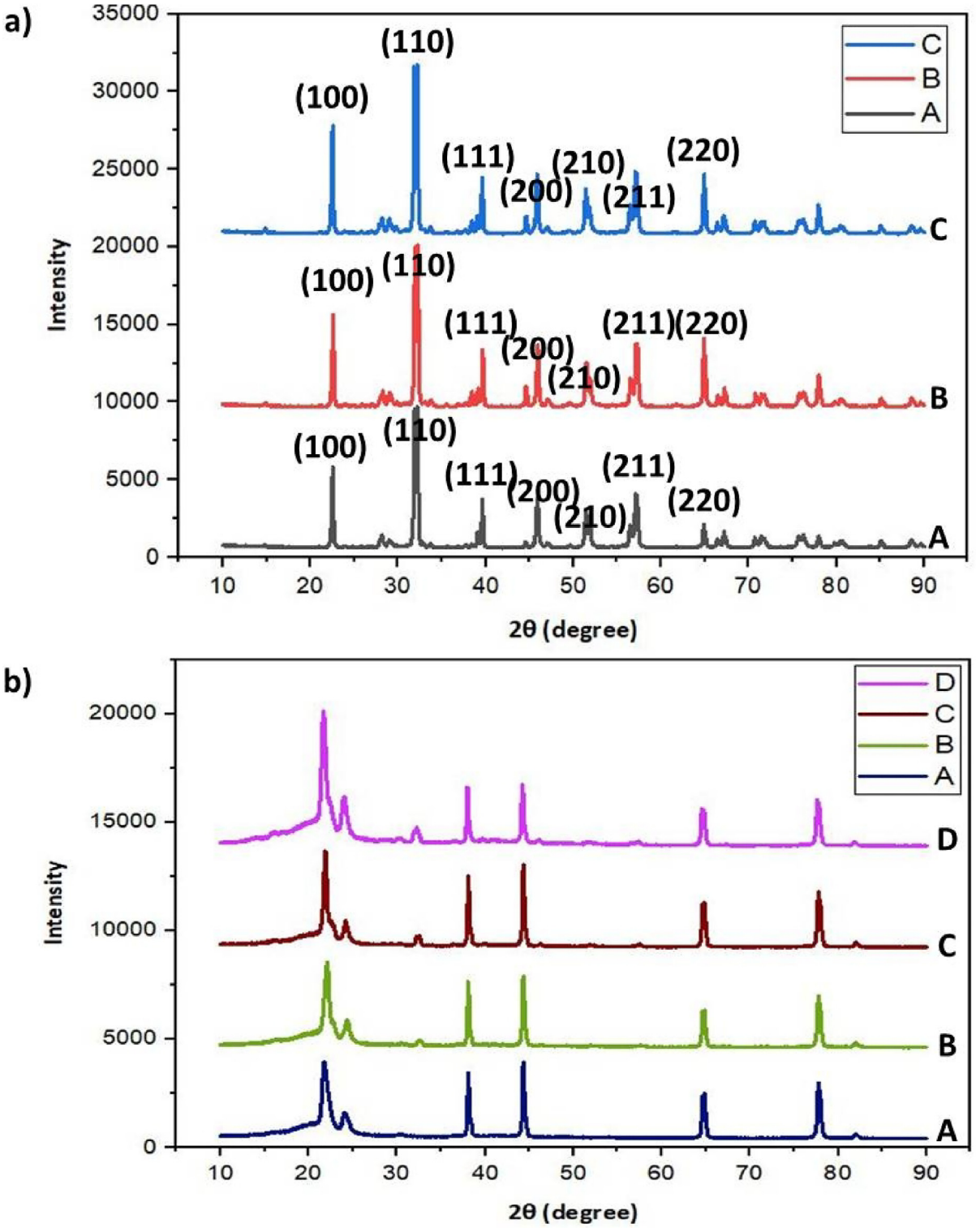

Fig. 5. X-ray diffractometer spectrums of the nanoparticles (a), and scaffolds (b).

dark. AC conductivity values of the samples between the frequencies 40 Hz-10 kHz were not presented because of the measurement limit of the LCZ meter. The results showed that ac conductivity values were affected by the pH values of the starting solutions as seen from the figure that ac conductivity of the scaffolds took placed greater than those of the pellets. Another observation on Fig. 6c that ac conductivity of the pellets and scaffolds were increased with increasing frequency. Frequency dependence of the samples was determined from the slope of the Log σ_{ac} − Log f curves.

Frequency dependence of the measured ac conductivity (Log σ_{ac} − Log f) of the pellets **PA**, **PB**, and **PC** and scaffolds **SU**, **SA**, **SB**, and **SC** can be represented by the universal power law. The universal power law is given by the Eq. (2) [32].

$$\sigma_{ac} = Aw^{s} \quad (2)$$

where ω is the angular frequency, A and s are material depended on

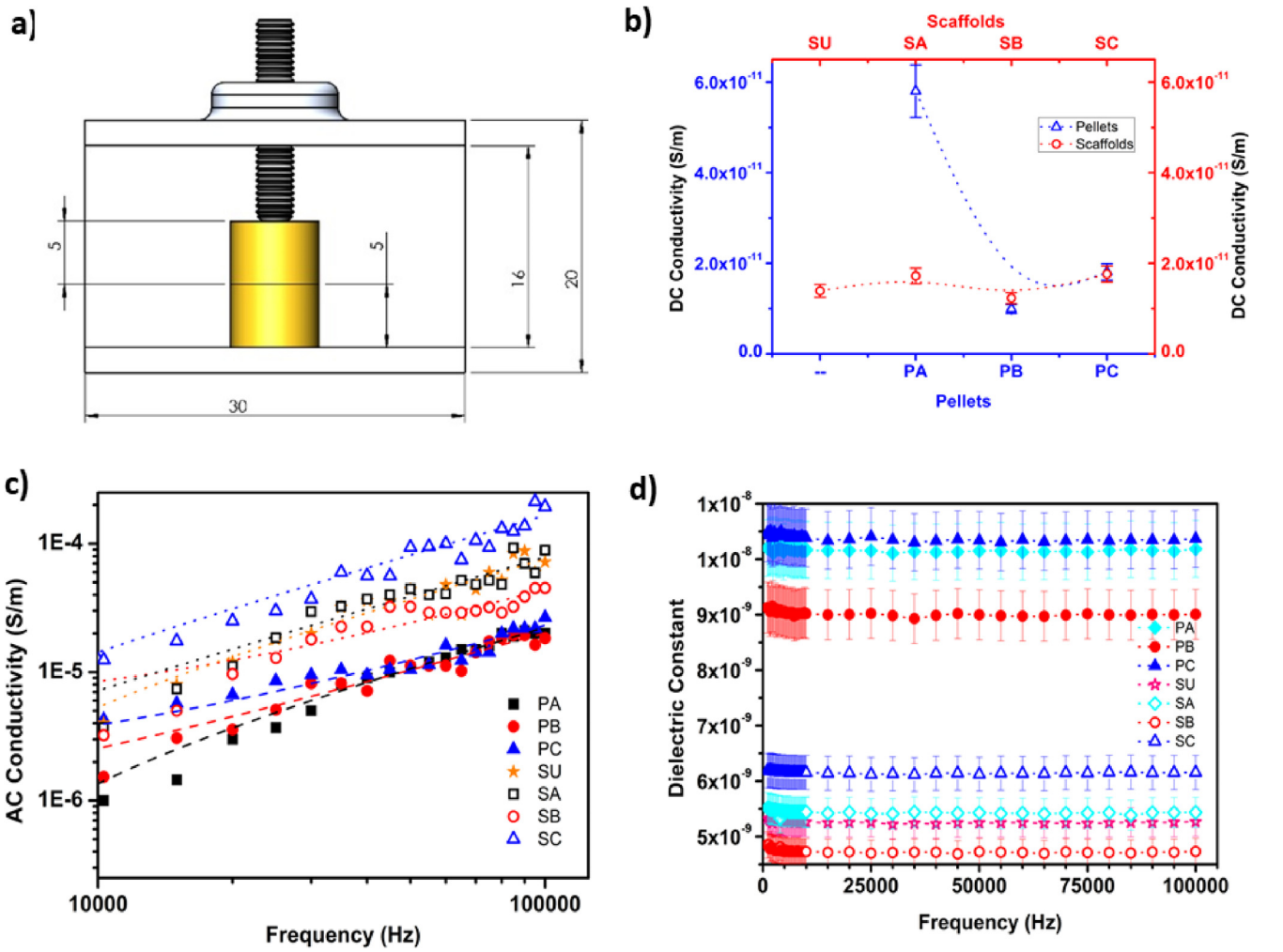

Fig. 6. Schematic view of the experimental setup of technique that provides to get electrical properties of the porous scaffolds (a), DC conductivity values (b), AC conductivity values (c), and dielectric constant values (d) of the pellets PA, PB, PC, and scaffolds SU, SA, SB, and SC at 295 K, in vacuum.

constants. S values can be calculated from the slopes of the curves given in Fig. 6c. The Magnitude of the s values was found as 2.37×10^{-13}, 1.92×10^{-13}, and 2.24×10^{-13} with regression coefficients 0.98, 0.91, and 0.91 for the pellets **PA**, **PB**, and **PC**, respectively. The values are 7.86×10^{-10}, 7.94×10^{-10}, 3.94×10^{-10}, and 1.68×10^{-9} with regression coefficients 0.83, 0.85, 0.86, and 0.95 for the scaffolds **SU**, **SA**, **SB**, and **SC**, respectively. Frequency dependence of the ac conductivity decreased as the pH value increased from 10.64 to 11.32 then increased toward pH 11.58. Similar behaviour was also obtained for the scaffolds.

To investigate the effects of the pH values of the starting solution of $BiFeO_3$ on the dielectric constant of the pellets and scaffolds, the capacitance of the samples were measured. To examine the frequency dependence of the dielectric constant, the measurements were also performed in the frequency range of 40 Hz–100 kHz. Fig. 6d showed a dielectric constant of the pellets and scaffolds at different frequencies in the measurement frequency range.

It was observed that dielectric constant values of the pellets were affected by pH values of the starting solutions of the $BiFeO_3$. The values were calculated as 10.19, 9.01, and 10.37 nF at 100 kHz for the pellets **PA**, **PB**, and **PC**, respectively. Dielectric constant values for the scaffolds were calculated as 5.27, 5.44, 4.73, and 6.16 nF at 100 kHz for the scaffolds **SU**, **SA**, **SB**, and **SC**, respectively. Maximum dielectric constant values were obtained for the pellets and scaffolds as 10.37 nF and 6.16 nF for the pellet **PC** (pH = 11.58) and for the scaffold **SC** (pH = 11.58), respectively. However, the dielectric constant of the samples nearly remained the same, but a slight decrease in dielectric constant was observed up to 10 kHz. Between the frequencies, 40 Hz–10 kHz, dielectric constant slightly decreased with an increasing frequency indicating dominant contribution to dielectric constant from interfacial polarization effect. After 10 kHz dielectric constant nearly remains the same, that can be interpreted as a steady-state [33] as can be seen from the Fig. 6d that dielectric constant of the undoped scaffold has a lower dielectric constant than that of $BiFeO_3$. After adding $BiFeO_3$ (pH = 10.64) dielectric of the composite were increased. The increase may be caused by an increased number of polarizable units. It is decreased when the undoped scaffold doped with $BiFeO_3$ (pH = 11.32). Then it raised again when the scaffold doped with $BiFeO_3$ (pH = 11.58). A possible explanation for the decrease can be explained as follows: the force due to electrostatic interactions of the doped nanoparticles constraints the molecular motion. Because of this, the dielectric polarization of the material reduces. Similar results were reported earlier [33]. Pellets **PA**, **PB**, and **PC** also showed similar behaviour.

The purpose of cell culture test was to find the capability of $BiFeO_3$ particles and scaffolds as a biomaterial for adenocarcinoma lung cancer. In Fig. 7, the cytotoxicity (MTT) tests indicated that particles and PCL-based composites had no cytotoxic compared to control. All results were statistically significant ($p < 0.05$). However, the particles and composites had no enhancing effect on cell proliferation. The decrease in cell viability can be overlooked. When the particles were compared among themselves, the viability value of the particle having a value of

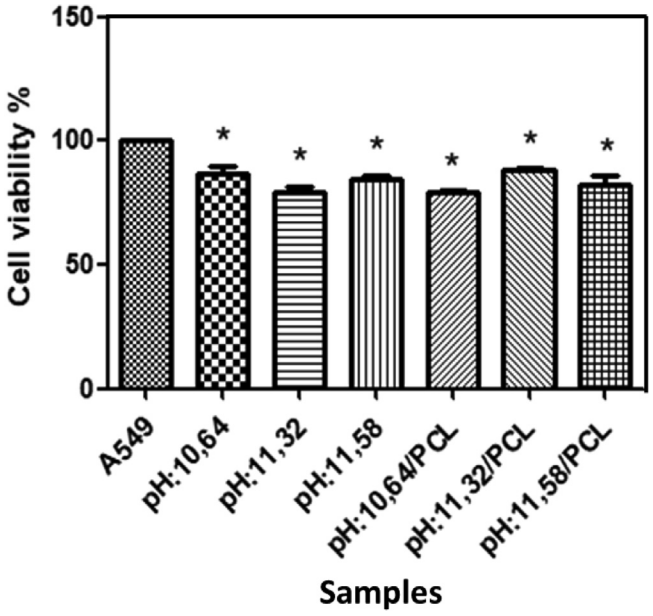

Fig. 7. Cell viability graph of the particles and scaffolds with a 2D cell line (A549).

10.64 was higher than others. However, there was not observed any trends to say with increasing pH value, the viability of particles was decreasing. When the viability of the 3D-printed scaffolds was examined, it was found that SB had the highest viability value in all. According to the results, it can be said that all nanoparticles and nanoparticles added scaffolds had no cytotoxicity and they can be used in biomedical applications, but further studies are required.

The confocal microscope enables to get the distribution of scaffolds and cells by using 3D images [34,35]. Fig. 8(a–d) showed the images of the scaffolds that were taken by a confocal microscope. As expected, the $BiFeO_3$ doped scaffolds had more cell density compared to the undoped scaffold after 3 days incubation. The nuclei, largest part of the cell, were seen clearly for $BiFeO_3$ doped scaffolds. Compared with $BiFeO_3$ added scaffolds, it can be said that the number of cells was higher for the pH value of 11.32, and the cell-cell interactions were seen clearly with their secretions.

To observe the adhesion ability of A549 cell line to 3D-printed scaffolds, the SEM device was used to focus on cell morphology. Adenocarcinoma is a cancer cell that originates in the glands, and they can have the ability to spread to other parts of the body. These cells can grow slow, so it is easy to found before it spreads from the lungs to the body [36]. In Fig. 9(a, b) and Fig. 9(c, d) the nearly round cell morphology on the scaffolds was seen clearly with its roots for SA and SB, respectively. In Fig. 9(e, f), cancer cell with a round shape was exactly

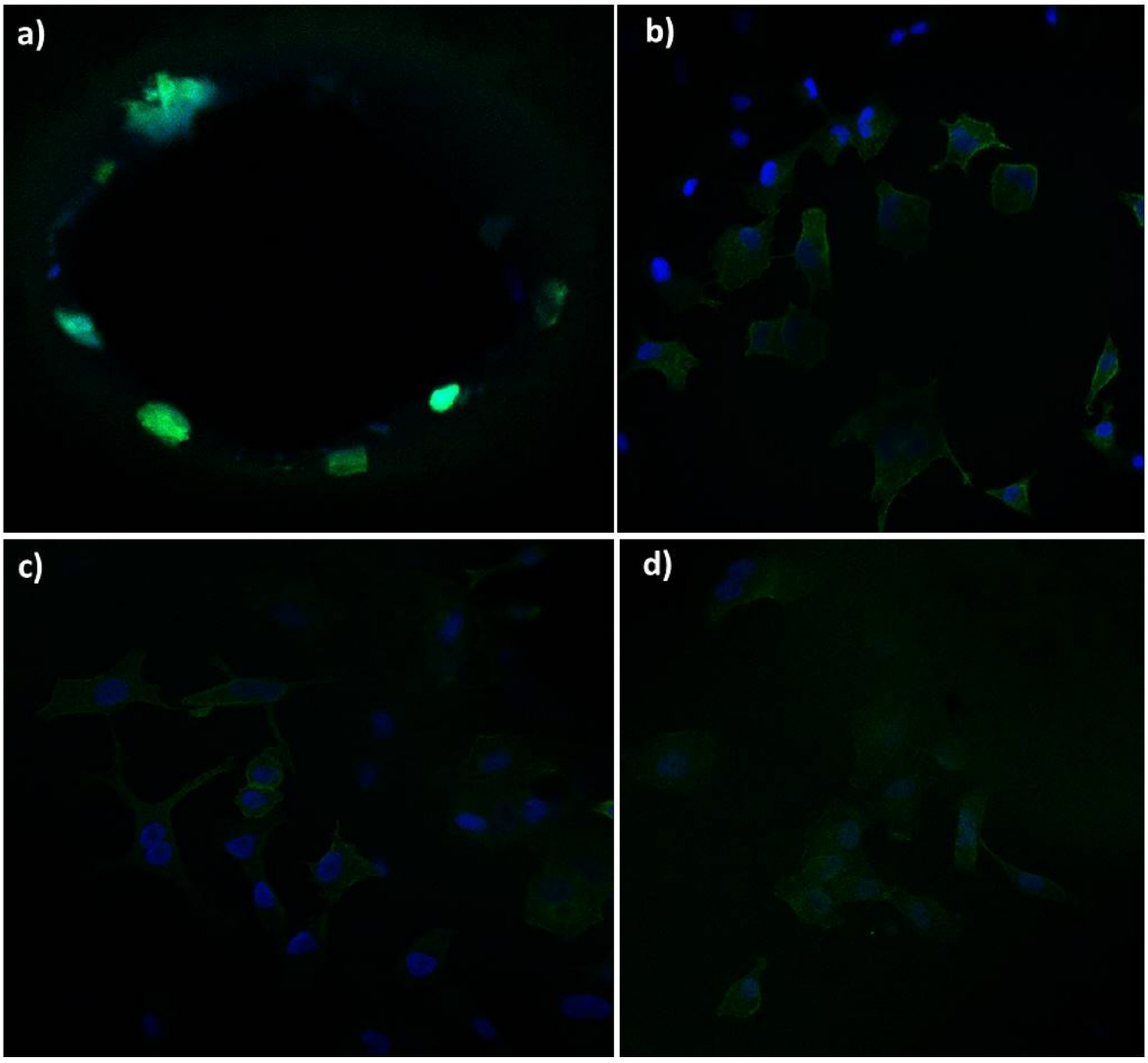

Fig. 8. Fluorescence images of SU (a), SA (b), SB (c), and SC (d) scaffolds at 20X magnification.

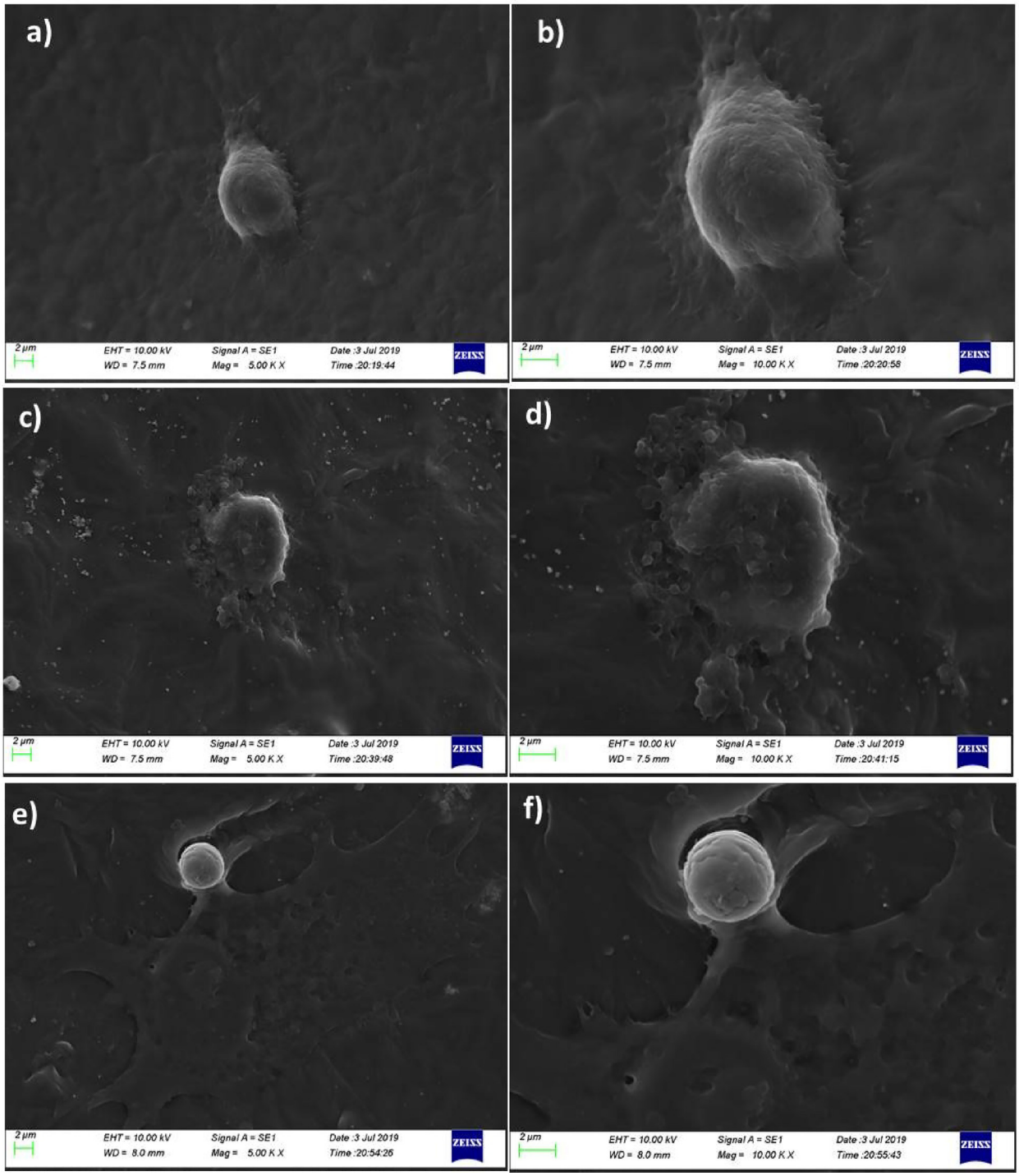

Fig. 9. The morphology of the A549 cell line on the 3D-printed scaffolds. SA (a), SB (b), and SC (c).

seen, and it is surrounded with its secretions which shows the spreading behaviour of the cells on the SC [37]. The secretions and cell morphology were more specific for SC than SA and SB. This might be due to the size of the nanoparticles. SC had the smallest particle size, which provides significant cell/material interaction [38].

The antibacterial potentials of the powders and discs were measured as the diameter of the zone around the powders and 3D-printed discs. Fig. 10(a–d) showed the antibacterial efficiencies of powders and Fig. 10(e–h) demonstrated the antibacterial activities of the PCL/$BiFeO_3$ scaffolds. Table 3 revealed that the inhibition zones appeared after 24–48 h incubation. PCL disc was used as a control group for comparing the antimicrobial activities of the scaffolds with three different pH values. According to the method used in this test, there was not observed any antimicrobial activity against the test microorganisms.

4. Conclusion

The $BiFeO_3$ nanoparticles were successfully synthesized with the co-precipitation method and added into the 25%PCL solutions to obtain 25%PCL/2%$BiFeO_3$ composites. The effects of pH on structural, dielectric, and biological properties of $BiFeO_3$ were examined for both nanoparticles and scaffolds. Crystallite sizes indicated from XRD analysis were found to be within 15–10 nm for nanoparticles and scaffolds

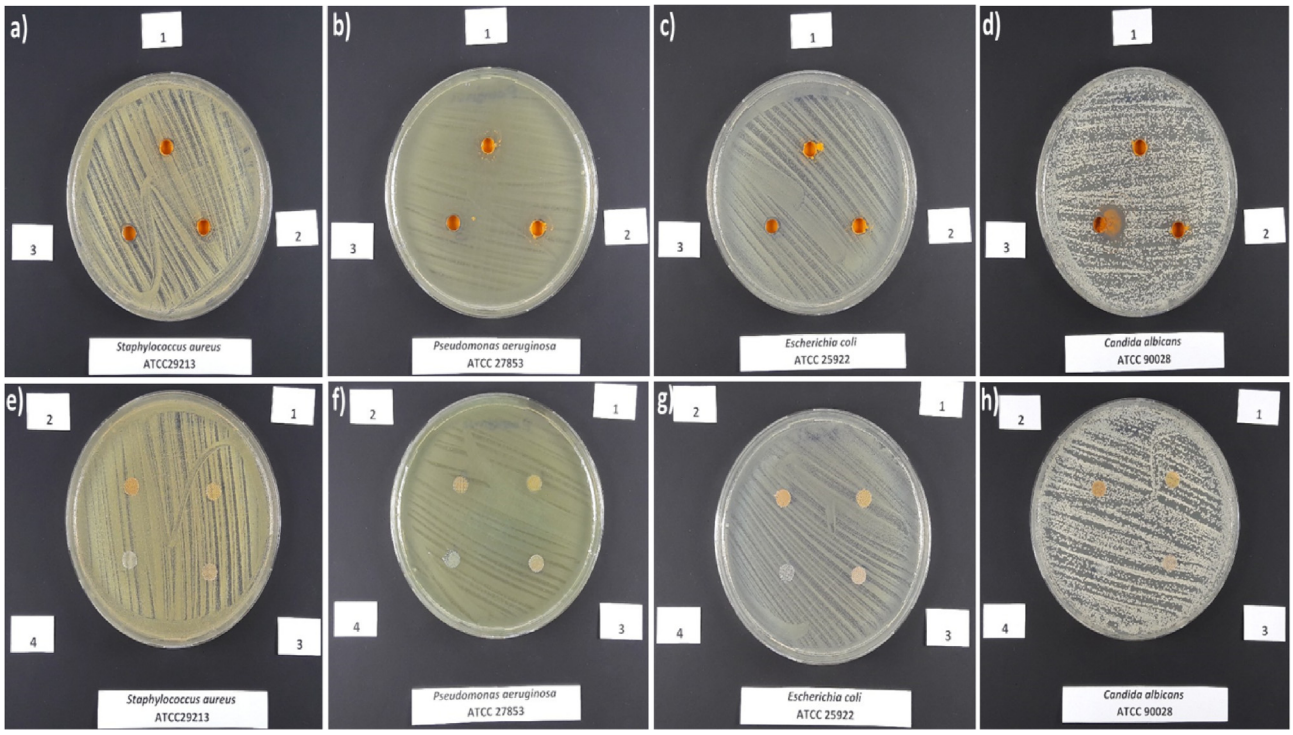

Fig. 10. The antibacterial activities of powders (a, b, c, and d) and scaffolds (e, f, g, and h).

Table 3
Antimicrobial activities of particles and scaffolds, M: Meropenem, A: Amphotericin B, E: Ethanol, DW: distilled water were not tested.

	Samples	Measured Zone Diameters (mm)			
		Staphylococcus aureus ATCC 29213	*Escherichia coli* ATCC 25922	*Pseudomonas aeruginosa* ATCC 27853	*Candida albicans* ATCC 90028
Discs	1	0	0	0	0
	2	0	0	0	0
	3	0	0	0	0
	4	0	0	0	0
	Disc M	**21.60**	**27.02**	**20.76**	–
Powders	1	0	0	0	0
	2	0	0	0	0
	3	0	0	0	0
	Canal M	**12.37**	**19.64**	**9.86**	–
	Canal A	–	–	–	**18.66**
	E	1	2	0	0
	DW	0	0	0	0

had nearly the same XRD pattern except for some shifts due to the $BiFeO_3$ addition with different pH values. According to the SEM images, the size of the nanoparticles was decreased generally with the increasing of the pH. The pore size of the scaffolds was measured and reported that by the $BiFeO_3$ addition, pore sizes were reduced compared to the control group. According to the antimicrobial and antifungal tests, no antibacterial effect was observed in both nanoparticles and scaffolds. The biocompatibility study of the synthesized nanoparticles and produced scaffolds were performed and found that samples had no toxic effect. From DC measurements, we can conclude that grain boundary resistance controls the electron flows along with the material. AC conductivity values of the pellets and scaffolds were found to be frequency depended. All the scaffolds studied showed greater conductivity values than that of the pellets. Dielectric constant values of the pellets and scaffolds nearly remained the same after 10 kHz, that can be interpreted as steady state. All the pellets showed greater dielectric constant values than all the scaffolds. The pellet and scaffold with pH 11.58 showed greater dielectric constant among the samples.

Declaration of Competing Interest

The authors declare that they have no known competing financial interests or personal relationships that could have appeared to influence the work reported in this paper.

Acknowledgements

The authors thank Dr. Ali Sahin for confocal images at Genetic and Metabolic Diseases Research Center (GEMHAM), Marmara University, Faculty of Medicine, Turkey. The authors also thank to Marmara University Scientific Research Committee (Project Numbers: FEN-C-YLP-090517-0286) for their financial support.

References

[1] W. Eerenstein, N.D. Mathur, J.F. Scott, Nature 442 (2006) 759–765.
[2] T.J. Park, G.C. Papaefthymiou, A.J. Viescas, A.R. Moodenbaugh, S.S. Wong, Nano Lett. 7 (2007) 766–772.
[3] J. Wang, J.B. Neaton, H. Zheng, V. Nagarajan, S.B. Ogale, B. Liu, D. Viehland, V. Vaithyanathan, D.G. Schlom, U.V. Waghmare, N.A. Spaldin, Science 299 (5613) (2003) 1719–1722.
[4] M.M. Kumar, V.R. Palkar, K. Srinivas, S.V. Suryanarayana, Appl. Phys. Lett. 76 (19) (2000) 2764–2766.
[5] G. Catalan, J.F. Scott, Adv. Mater. 21 (2009) 2463–2485.
[6] H. Sangian, O. Mirzaee, M. Tajally, ACERP 32 (1) (2017) 31–36.
[7] K. Biswas, D. De, J. Bandyopadhyay, N. Dutta, S. Rana, P. Se, S.K. Bandyopadhyay, P.K. Chakraborty, Mater. Chem. Phys. 195 (2017) 207–212.
[8] D. Staedler, S. Passemard, T. Magouroux, A. Rogov, C.M. Maguire, B.M. Mohamed, S. Schwung, D. Rytz, T. Jüstel, S. Hwu, Y. Mugner, R.L. Dantec, Y. Volkov, S. Gerber-Lemaine, A. Prrina-Mello, L. Bonacina, J.P. Wolf, Nanomedicine 11 (4) (2015) 815–824.
[9] A. Manzoor, A.M. Afzal, M. Umair, A. Ali, M. Rizwan, M.Z. Yaqoob, J. Magn. Magn. Mater. 393 (2015) 269–272.
[10] H. Xie, K. Wang, Y. Jiang, Y. Zhao, X. Wang, Met.-Organ. Nano-Met. Chem. 44 (9) (2014) 1363–1367.
[11] M. Muneeswaran, P. Jegatheesan, N.V. Giridharan, J. Exp. Nanosci. 8 (3) (2013) 341–346.
[12] C. Yang, Y. Chen, W. Guo, Y. Gao, C. Song, Q. Zhang, N. Zheng, X. Han, C. Guo, Adv.

Funct. Mater. 28 (1706827) (2018) 1–13.
[13] A.V. Rane, K. Kanny, V.K. Abitha, S. Thomas, Elsevier (2018) 121–139.
[14] E. Malikmammadov, T.E. Tanir, A. Kiziltay, V. Hasirci, N. Hasirci, J. Biomater. Sci. Polym. Ed. 29 (2019) 863–893.
[15] B. Azimi, P. Nourpanah, M. Rabiee, S. Arbab, J. Eng. Fibers Fabr. 9 (3) (2014) 74–90.
[16] M. Hashim, Alimuddin, S. Kumar, J. Alloys Compd. 511 (1) (2012) 107–114.
[17] Z.R. Ege, A. Akan, F.N. Oktar, C.C. Lin, D.S. Kuruca, B. Karademir, Y.M. Sahin, G. Erdemir, O. Gunduz, J. Biomed. Mater. Res. Part B: Appl. Biomater. 14 (5) (2019) 538–554.
[18] T. Mosmann, J. Immunol. Meth. 65 (1983) 55–63.
[19] C. Perez, M. Pauli, P. Bazerque, Acta Biol. Med. Exp. 15 (1990) 113–115.
[20] M. Sakar, S. Balakumar, P. Saravanan, S.N. Jaisankar, Mater. Res. Bull. 48 (2013) 2878–2885.
[21] O.P. Bajpai, J.B. Kamdi, M. Selvakumar, S. Ram, D. Khastgir, S. Chattopadhyay, Express Polym. Lett. 8 (9) (2014) 669–681.
[22] M.N. Abdillah, D. Triyono, International Conference on Mathematics and Natural Sciences (ICMNS), 1245, 012087, 1-9, (2019).
[23] J. Ma, L. Lin, Y. Zuo, Q. Zou, X. Ren, J. Li, Y. Li, RSC Adv. 9 (2019) 5338–5346.
[24] S.K. Srivastav, N.S. Gajbhiye, J. Am. Ceram. Soc. 95 (2012) 1–5.
[25] D.C. Jia, J.H. Xu, H. Ke, W. Wang, Y. Zhou, J. Eur. Ceram. Soc. 29 (2009) 3099–3103.
[26] S. Godara, N. Sinhaa, G. Raya, B. Kumar, J. Asian Ceram. Soc. 2 (2014) 416–421.
[27] H. Jensen, J.H. Pedersen, J.E. Jorgensen, J.S. Pedersen, K.D. Joensen, S.B. Iversen, E.G. Sogaard, J. Exp. Nanosci. 1 (3) (2006) 355–373.
[28] M. Borjigin, C. Eskridge, R. Niamat, B. Strouse, P. Bialk, E.B. Kmiec, Int. J. Nanomed. 8 (2013) 855–864.
[29] C. Guang-Mei, Z. Tie-Mei, C. Lei, H. Yi-Ping, Asian J. Chem. 22 (8) (2010) 5902–5912.
[30] K.L.L. Maldonado, P. de la Presa, M.A. de la Rubia, P. Crespo, J. de Frutos, A. Hernando, J.A. Matutes Aquino, J.T. Elizalde Galindo, J. Nanopart. Res. 16 (2014) 2482.
[31] W. Sukbua, J. Muangban, N. Triroj, P. Jaroenapibal, Proc. Eng. 47 (2012) 370–373.
[32] M. Pollak, T.H. Geballe, Phys. Rev. 122 (1961) 1742–1754.
[33] S. Choudhary, Phys. B 522 (2017) 48–56.
[34] S.W. Paddock, Mol. Biotechnol. 16 (2000) 127–149.
[35] W. Song, W. Liu, X. Niu, Q. Wang, L. Sun, M. Liu, Y. Fan, Microsc. Res. Technol. 76 (2013) 1154–1162.
[36] C. Zappa, S.A. Mousa, Transl. Lung Cancer Res. 5 (3) (2016) 288–300.
[37] A.A. Ahmed, C.J. Luo, S. Perez-Garrido, C.R. Browse, C. Thrasivoulou, S.D. Stoyanov, S.K. Smoukov, I. Gout, Biotechnol Prog. 35 (2019) 1–13.
[38] M.A. Islam, S. Barua, D. Barua, BMC Syst. Biol. 11 (113) (2017) 1–13.